Localized mesosphere-stratosphere-troposphere radar echoes from the *E* region at 69°N: Properties and physical mechanisms

Markus Rapp,[1] Lasse Leitert,[1] Ralph Latteck,[1] Marius Zecha,[1] Peter Hoffmann,[1] Josef Höffner,[1] Ulf-Peter Hoppe,[2] Cesar La Hoz,[3] and Eivind V. Thrane[4]

Received 1 October 2010; revised 5 November 2010; accepted 14 December 2010; published 25 February 2011.

[1] We present the first observations, to our knowledge, of a new class of high-latitude mesosphere-stratosphere-troposphere radar echoes from the *E* region as observed with the Arctic Lidar Observatory for Middle Atmosphere Research wind radar during the period 2004–2008. These echoes occur primarily during the summer months and in the altitude range from 93 to 114 km, with a pronounced peak of maximum occurrence at about 100 km. The echoes are rather short with typical durations of ~20 min, with some examples lasting as long as 3 h. The echoes typically cover only a few hundred meters in the vertical and show both small Doppler velocities (±1–2 m/s) as well as very narrow spectral widths (just a few meters per second when converted to Doppler velocities). The echoes are highly aspect sensitive indicative of a specular-scattering mechanism and reveal a distinct diurnal variation with maxima of occurrence around noon and midnight. The latter is related to the semidiurnal tidal components of the zonal and meridional wind where times of occurrence correspond to large values of corresponding vertical wind shears. Considering possible physical mechanisms, turbulence with large Schmidt number scatter is likely ruled out as is auroral backscatter. Finally, a strong case for a close correspondence of the echoes to sporadic *E* layers is presented on the basis of comparisons to ionosonde data, occurrence patterns of sporadic layers, simultaneous and common volume lidar measurements of a sporadic Fe layer, as well as simultaneous measurements of sporadic *E* layers with the European Incoherent Scatter UHF radar at a horizontal distance of 130 km. Applying the theory of partial reflections to the observed electron density gradients, we are able to demonstrate that the observed echo strengths can likely be explained on the basis of this scattering mechanism.

Citation: Rapp, M., L. Leitert, R. Latteck, M. Zecha, P. Hoffmann, J. Höffner, U.-P. Hoppe, C. La Hoz, and E. V. Thrane (2011), Localized mesosphere-stratosphere-troposphere radar echoes from the *E* region at 69°N: Properties and physical mechanisms, *J. Geophys. Res.*, *116*, A02320, doi:10.1029/2010JA016167.

1. Introduction

[2] Mesosphere-stratosphere-troposphere (MST) radars which are typically operated at frequencies of about 50 MHz are powerful tools to study the structure and dynamics of the troposphere and lower stratosphere (~0–20 km altitude) as well as the mesosphere/lower thermosphere (MLT) region [*Woodman and Guillen*, 1974; *Hocking*, 2011]. At polar latitudes two main types of echoes have received considerable scientific interest over the past 30 years. These are the so-called polar mesosphere summer echoes (PMSE) which occur during the summer months in the altitude range from 80–90 km (see *Cho and Kelley* [1993] and *Rapp and Lübken* [2004] for suitable reviews) and the so-called polar mesosphere winter echoes (PMWE) which primarily (though not exclusively) occur during the winter months in the entire midmesosphere from 55–85 km altitude [e.g., *Kirkwood et al.*, 2002; *Zeller et al.*, 2006]. Both echo types were first discovered in the end of the 1970s by *Ecklund and Balsley* [1981] and *Czechowsky et al.* [1979] at high latitudes and midlatitudes, respectively.

[3] PMSE are today known to be closely related to the properties of ice particles which form in the extreme thermal environment of the polar summer mesopause region where mean minimum temperatures of ~130 K and less are attained [*Havnes et al.*, 1996; *Lübken*, 1999]. The theory with currently largest acceptance in the community assumes that these echoes originate from neutral air turbulence in combination with a reduced electron diffusivity. The latter is expected due to the presence of charged ice aerosol particles such that structures in the radar refractive index (determined

[1]Leibniz-Institute of Atmospheric Physics at University of Rostock, Kühlungsborn, Germany.
[2]Norwegian Defense Research Establishment, Kjeller, Norway.
[3]Department of Physics, University of Tromsø, Tromsø, Norway.
[4]Andøya Rocket Range, Andenes, Norway.

0148-0227/11/2010JA016167

by the electron density at mesospheric altitudes) can exist and prevail at spatial scales of half the radar wavelength such that the condition for Bragg scattering is fulfilled [e.g., *Kelley et al.*, 1987; *Cho et al.*, 1992; *Rapp and Lübken*, 2003; *Lie-Svendsen et al.*, 2003; *Nicolls et al.*, 2008; *Li et al.*, 2010; *Varney et al.*, 2011].

[4] In contrast to the case of PMSE, the physical mechanism leading to PMWE is currently strongly debated. On the one hand, *Lübken et al.* [2006], *Brattli et al.* [2006], and *Lübken et al.* [2007] presented results from in situ and radar measurements of turbulence, temperatures, and electron densities within PMWE observed with a 50 MHz radar and showed quantitatively that the studied echoes were consistent with the assumption of Bragg scattering from fluctuations that were directly created by neutral air turbulence as discussed by *Hocking* [1985]. On the other hand, *Belova et al.* [2005] presented PMWE with the European Incoherent Scatter (EISCAT) VHF radar operating at 224 MHz and concluded that the echoes observed at this much larger frequency and hence considerably smaller Bragg wavelength (i.e., 67 cm in contrast to 3 m for a 50 MHz radar) were at least 2 orders of magnitude too strong to be explained by a pure turbulence-related scattering mechanism as suggested by *Lübken et al.* [2006]. Also, *Kirkwood et al.* [2006] presented PMWE observations with the ESRAD 50 MHz MST radar showing that on some occasions the scatterers responsible for PMWE showed very large horizontal propagation speeds close to the speed of sound. On the basis of these very large velocities, *Kirkwood et al.* [2006] proposed that PMWE originate from highly damped ion-acoustic waves generated by partial reflection of infrasonic waves. Finally, *La Hoz and Havnes* [2008] recently presented results of active RF-heating experiments in PMWE and concluded that the observed signatures indicated the involvement of charged nanometer-scale particles much like in the case of PMSE. Since such charged particles of likely meteoric origin have indeed been observed with various techniques in recent years (see, e.g., *Friedrich and Rapp* [2009] for a recent review), it thus appears likely that charged aerosol particles indeed play some role in the generation of PMWE. However, the details of the scattering mechanism(s) are obviously not yet completely understood and will require more attention in the future.

[5] Besides PMSE and PMWE which are regularly observed with MST radars at polar latitudes, there is one further class of echoes from the polar *E* region which have, however, only been reported once and appear to have not been observed since these initial observations. These are the observations of *Rüster and Schlegel* [1999], who reported echoes at altitudes between 90 and 105 km, observed with the Arctic Lidar Observatory for Middle Atmosphere Research (ALOMAR) SOUSY radar operating at 53 MHz. This is the altitude range where usually only coherent echoes from field-aligned irregularities are expected. Such echoes should not be observable with a vertically pointed MST radar at the polar location of ALOMAR (69°N, 16°E) where the Earth's magnetic field has a declination of 77°. Field-aligned irregularities are generally thought to be caused by the Farley-Buneman and/or gradient drift instability (see, e.g., *Haldoupis* [1989] for a review). However, after detailed discussion, *Rüster and Schlegel* [1999] concluded that their observations could not be explained by these mechanisms and that other alternative processes need to be invoked. One such alternative was presented by *Robinson and Schlegel* [2000], who proposed a new instability mechanism based on field-aligned electron drifts with additional positive feedback from electron collisional heating. Realizing that their theory predicted, however, only waves in excess of a few tens of meters, *Robinson and Schlegel* [2000] further speculated about additional nonlinear feedback mechanisms that could possibly shift the the wavelength range of the instability to the required value of ~3 m. However, since the observations of *Rüster and Schlegel* [1999] were never repeated such that no additional observational constraints are available, it remains an open question whether or not the mechanisms proposed by *Robinson and Schlegel* [2000] do occur and lead to detectable radar echoes.

[6] In the current manuscript, we will present echoes from the 95–115 km altitude range observed with the ALWIN MST Radar which is the successor of the ALOMAR SOUSY radar and is also located in the vicinity of the ALOMAR observatory, i.e., at 69°N, 16°E. These echoes are entirely different from the ones reported by *Rüster and Schlegel* [1999] in that they are extremely narrow in vertical extent (see below). To the best of our knowledge such echoes have never been reported before.

[7] The structure of this article is as follows: In section 2 we briefly introduce the experimental details and then proceed to present typical examples of the observed echoes. Section 3 describes some statistical properties of the echoes as derived from a total of 5 years of observations, i.e., from 2004–2008. This is followed by a detailed discussion of our observations in section 4 in terms of possible scattering mechanisms. These include turbulence-related scatter, scatter from field-aligned irregularities, as well as partial reflections from large electron density gradients related to sporadic *E* layers. Finally, our main conclusions are presented in section 5.

2. Observations

[8] The observations described here were obtained with the ALOMAR-wind VHF radar (ALWIN) during the years 2004–2008. The ALWIN VHF radar has been described in detail by *Latteck et al.* [1999] and additional information about the absolute calibration of the radar has been presented by *Latteck et al.* [2007, 2008]. In short, the ALWIN VHF radar was a phased array consisting of 144 3-element Yagi antennas which was operated at a frequency of 53.5 MHz and transmitted a peak power of 36 kW with a half power full beam width of 6°. Note that operation of the ALWIN VHF radar already commenced in October 1998, however, it was not until 2004 that the sampled altitude range was extended from 50–94 to 50–114 km (with an effective pulse width of 300 m) in order to search for echoes of the type reported by *Rüster and Schlegel* [1999]. Further technical details of the radar as well as of the conducted experiments are provided in Table 1. Observations were sequentially made in the zenith, and pointing to 7 degrees off-zenith toward NW, NE, SE, and SW after which the sequence started from the beginning. As a result, the time resolution of the power profiles presented here is about 3 min (173 s).

[9] Figure 1 shows three examples of observations obtained in May and June 2008. Each of the three panels

Table 1. Technical Parameters of the ALWIN Radar as Well as the Experiments

	System Parameters	
Frequency	Power	Height Resolution
53.5 MHz	36 kW	300 m
	Experiment Parameters	
Height range	50.1–114 km	
PRF	1250 Hz	
Coherent integrations	64	
Delta t	0.0512 s	
Data points in time series	512	
Length of time series	26.2 s	
Nyquist frequency	19.53 Hz (−9.3 Hz.. +9.3 Hz)	
Nyquist velocity	54.75 m/s (−27.4 m/s.. +27.4 m/s)	
Code	complementary code	
Code length	8 bit	
Beam directions	5 (vertical and 7 deg off-zenith in NE, SW, SE, NW)	
Time resolution	173 s	

shows height-time-intensity (HTI) plots of the recorded echo power. In each of the three examples, the ALWIN VHF radar recorded PMSE from altitudes between 80–90 km as expected for this time of the year at the given location (see, e.g., *Latteck et al.* [2008] for details regarding the statistics of PMSE observed at ALOMAR). Interestingly, ALWIN also recorded an echo at about 75 km altitude at ~10 UT on 26 May which cannot be interpreted as PMSE unless the thermal structure was very different from its normal state. The average temperature at this altitude is 196 K which is approximately 46 K too warm to allow the existence of ice particles [*Lübken*, 1999]. Hence, this echo should rather be regarded as a "PMWE-type" echo even though this observation was obviously not obtained under polar winter conditions.

[10] In any case, the echoes of interest here are the ones observed for example at altitudes of 102–106 km from 20:30–22:00 UT on 26 May, at altitudes between 108–112 km from 20:00–21:00 UT on 27 May, and at altitudes of 96–100 km from 00:00–03:00 UT and from 11:00–14:00 UT on 14 June. In all of these examples the echoes are very narrow in vertical extent and cover 3 range gates of 300 m width at most. The echoes are very dynamic in the sense that they change altitude rapidly over time; that is, they show typical descent or ascent speeds of about 1–2 m/s.

[11] In order to scrutinize this behavior further we have also considered corresponding radial velocities and spectral widths (FWHM) derived from these observations. The corresponding results for two examples on 14 June and 5 July are presented in Figure 2. These samples show that the descent or ascent motion of the echoes with speeds of a few meters per second is quantitatively matched by corresponding radial (vertical since the radar beam was pointed vertically) velocities. We note that 1–2 m/s are typical vertical wind speeds at these altitudes as expected from gravity waves [e.g., *Hoppe and Hansen*, 1988]. We also note that observed spectral widths are very narrow with values in the range between 1–3 m/s (after conversion to Doppler velocity by multiplication with half the radar wavelength).

[12] Finally, we also considered whether the echoes presented here were also observed in the off-zenith directions when the ALWIN radar beam was pointed to a total of four different off-zenith positions with a zenith angle of 7°. Figure 3 shows corresponding height-time-intensity plots for five different beam directions for the particularly long-duration events on 14 June 2008. While the echoes in the zenith beam are continuously observed for two periods of about 3 h each, no corresponding sign is found in the off-zenith directions. This implies a rather strong aspect sensitivity of the echoes with a lower bound of −23 dB/7 deg or about −3 dB/deg (i.e., the maximum SNR in the zenith is ~20 dB which drops to the detection limit of about −3 dB in the off-zenith direction). We note that the rather long duration of these events of almost 3 h argues against spatial inhomogeneities as an alternative explanation for the large differences seen between the zenith and off-zenith beam direction.

3. Statistical Properties

[13] As a next step, we now consider the statistical properties of the echoes introduced above. For this purpose, we considered all ALWIN observations from the beginning of 2004 (when the altitude range was extended to 114 km, see above) to the end of 2008 (after which the radar was replaced by a new instrument). For each day, SNR plots were created and inspected visually to detect *E* region echoes in the 92–114 km altitude range. An echo was identified as such when part of the echo extended at least 5 dB above the noise level and consisted of several coherent points in order to distinguish them from meteor echoes. When a corresponding echoing structure was identified, an SNR of −3 dB was taken as the minimum SNR to be counted as belonging to an echo region. As a result of this procedure, a total of 59 h of such echoes was detected during all 5 years. Interestingly, the echo occurrence increased steadily from 2004 to 2008 with just 0.5 h of echoes in 2004, 4.5 h in 2005, 5 h in 2006, 11.5 h in 2007 and a record of 37.25 h in 2008. Based on these data, histograms for various parameters were computed and are presented below.

[14] To start with, Figure 4 shows the relative occurrence of echoes (i.e., normalized to 1) as a function of time of year and altitude. Figure 4 reveals both a strong seasonal variation as well as a pronounced altitude variation: The vast majority of events occurs between week 20 and 33, i.e., between mid-May and end of August with only some occasional events outside the summer season in October and January. Versus altitude, the echo occurrence shows a pronounced peak at about 100 km and covers the entire altitude range from 93 to 114 km.

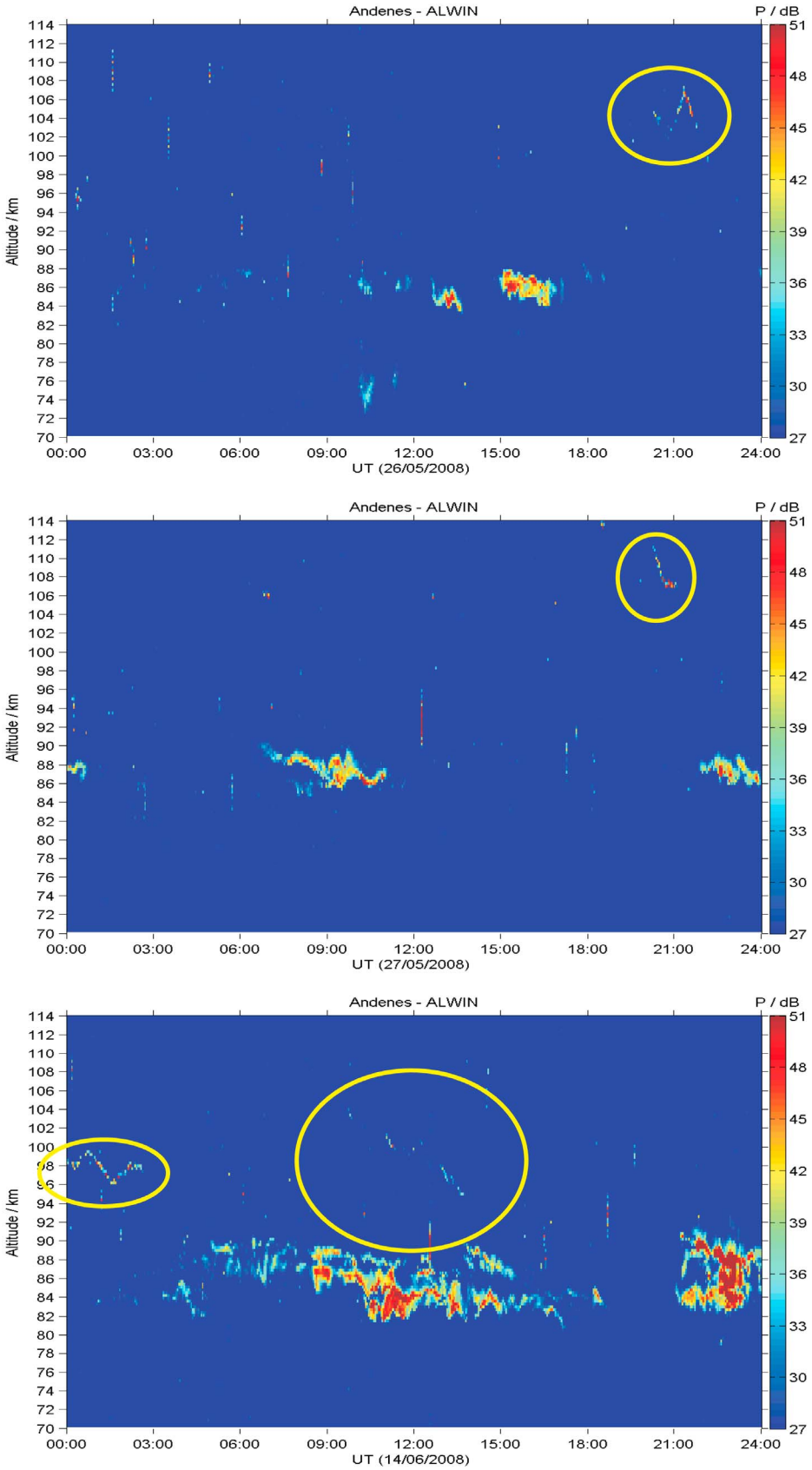

Figure 1. Height-time-intensity plots of radar echoes observed with the ALWIN MST radar on 3 different days in May and June 2008. The echoes under consideration are encircled in yellow.

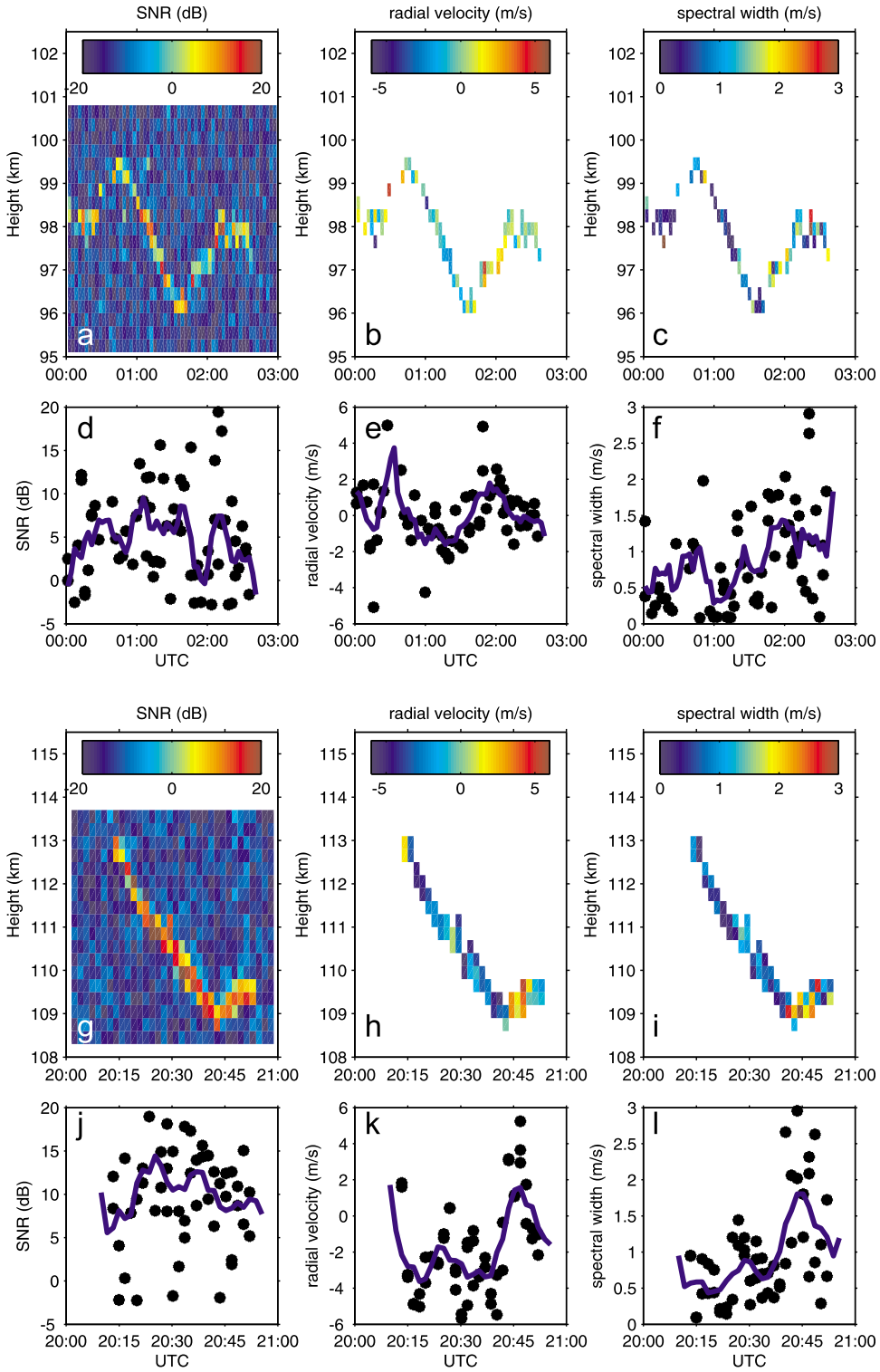

Figure 2. Signal-to-noise ratios (SNR), radial velocities, and spectral widths of two samples of echoes observed on (a–f) 14 June and (g–l) 5 July 2008, respectively. Figures 2a–2c and Figures 2g–2i show the data as height-time-intensity plots, whereas Figures 2d–2f and Figures 2j–2l show the values of SNR, radial velocity, and spectral width in the observed layer as a function of time. Dots represent single data points, and blue lines show five-point running means.

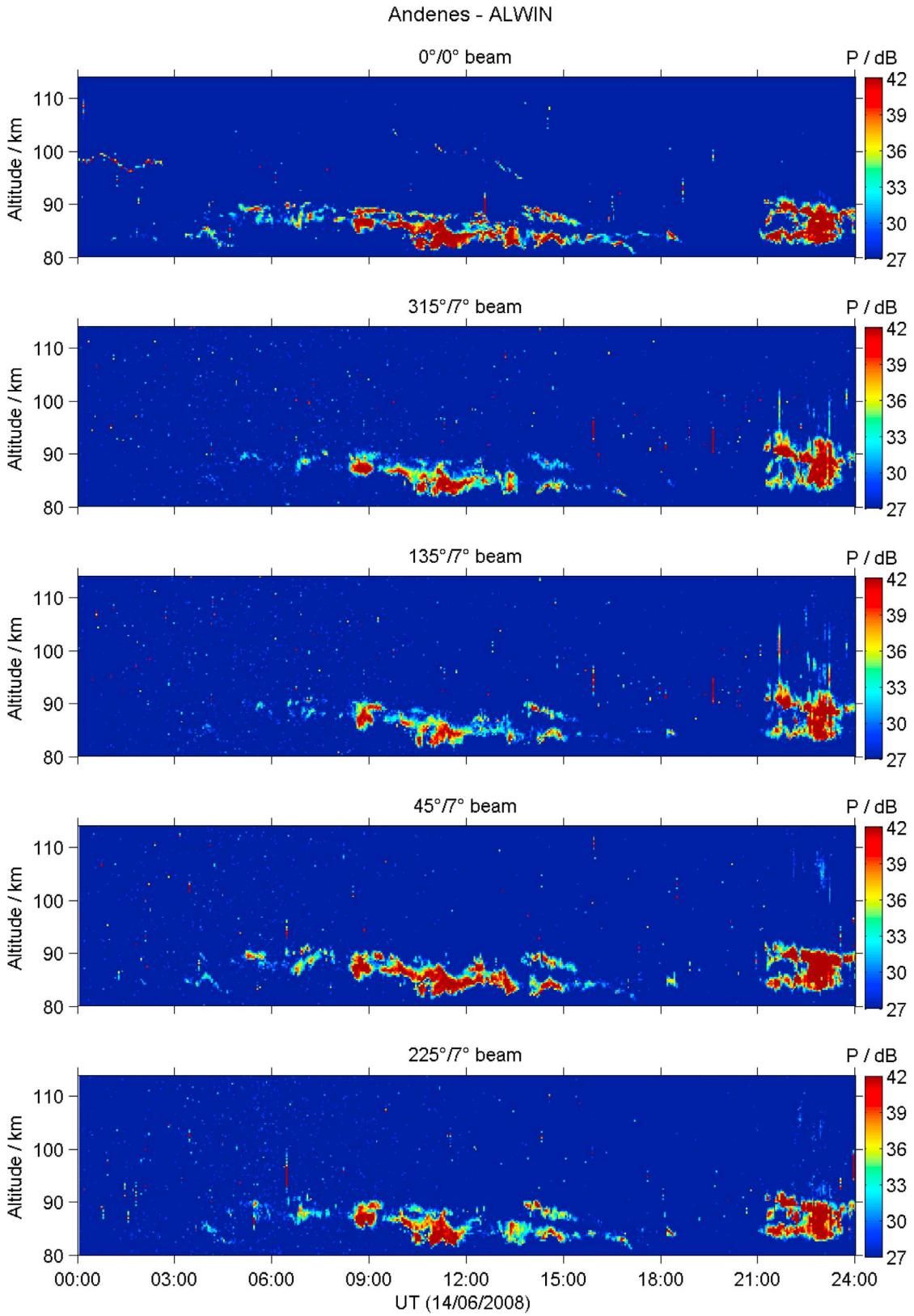

Figure 3. Height-time-intensity plots of radar echoes observed on 14 June 2008 in five different beam directions.

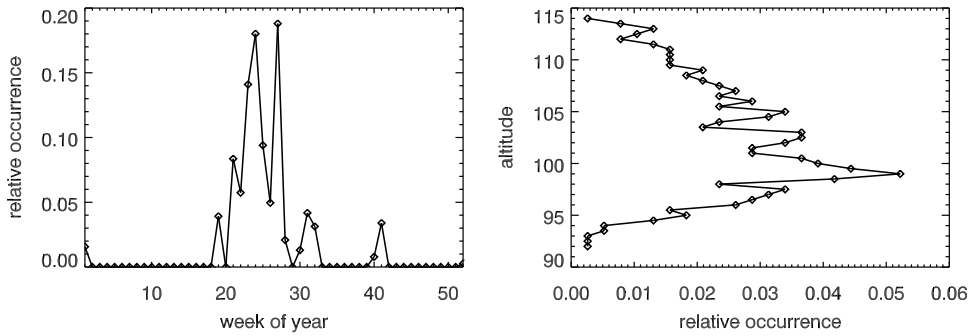

Figure 4. Relative occurrence of observations (normalized to 1) during the years 2004–2008 as (left) a function of time of year (in weeks) and as (right) a function of altitude.

[15] Considering next the temporal and vertical extent of the echoes, Figure 5 shows that most of the echoes are rather short lived with durations of less than or equal to 20 min with 90% of all observations revealing durations of less than or equal to 1 h and 20 min. As for the vertical extent, we see that more than 90% cover only one or two range gates of 300 m and no echoes are observed that cover more than three range gates.

[16] Next we turn to the distributions of SNR, radial velocity, and spectral widths. Corresponding results are presented in Figure 6. Figure 6 reveals that the SNR of the echoes peaks at the smallest values considered and that the relative occurrence of the SNR decreases approximately linearly with increasing SNR in dB. The corresponding histogram for radial (vertical) velocities shows a symmetric distribution around a mean negative velocity of ~−1 m/s with a FWHM of ~6 m/s. We argue below that this distribution is likely explained by a mean downward motion owing to the semidiurnal tide with superimposed gravity wave variations leading to both positive as well as negative variations with typical values in the ±3 m/s range. Furthermore, the distribution of spectral widths shows that more than 50% of all observations show extremely narrow spectra with widths of less than or equal to 1 m/s and about 90% with widths of less than or equal to 3 m/s.

[17] Finally, we also considered whether the echo occurrence shows any distinct diurnal variation pattern. For this purpose, the data were binned in 30 min intervals from 0–24 UT and 0.5 km altitude bins from 92 to 114 km. Resulting absolute numbers of echo occurrences are presented in Figure 7. Surprisingly, Figure 7 shows a distinct semidiurnal variation of the echo occurrence with echoes starting at high altitudes at ~5 and 17 UT and then propagating downward at a rate of about 0.5–1 m/s. Interestingly, this descent rate of echo occurrence is approximately the same as the average radial velocity of the echoes seen in Figure 6.

[18] In order to test whether this semidiurnal variation is in any way related to the variation of the semidiurnal tide, we compared the echo occurrence pattern to zonal and meridional wind variations derived from observations with the collocated ALOMAR Meteor radar [e.g., *Hoffmann*

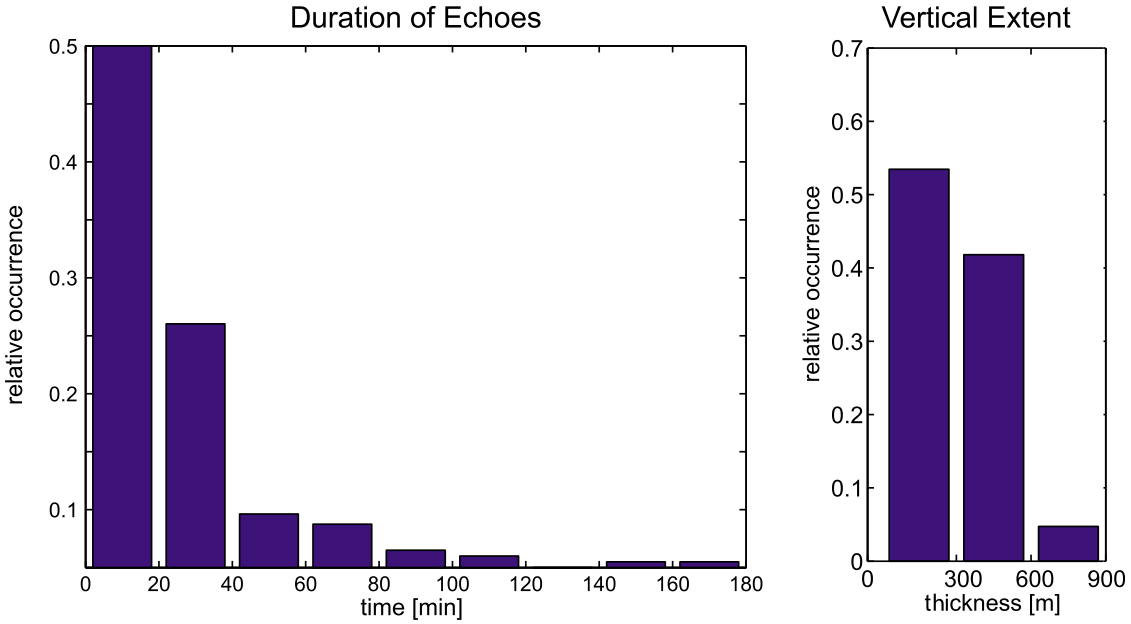

Figure 5. (left) Histogram of the duration of observed echoes. (right) Histogram of the observed vertical extent of observed echoes.

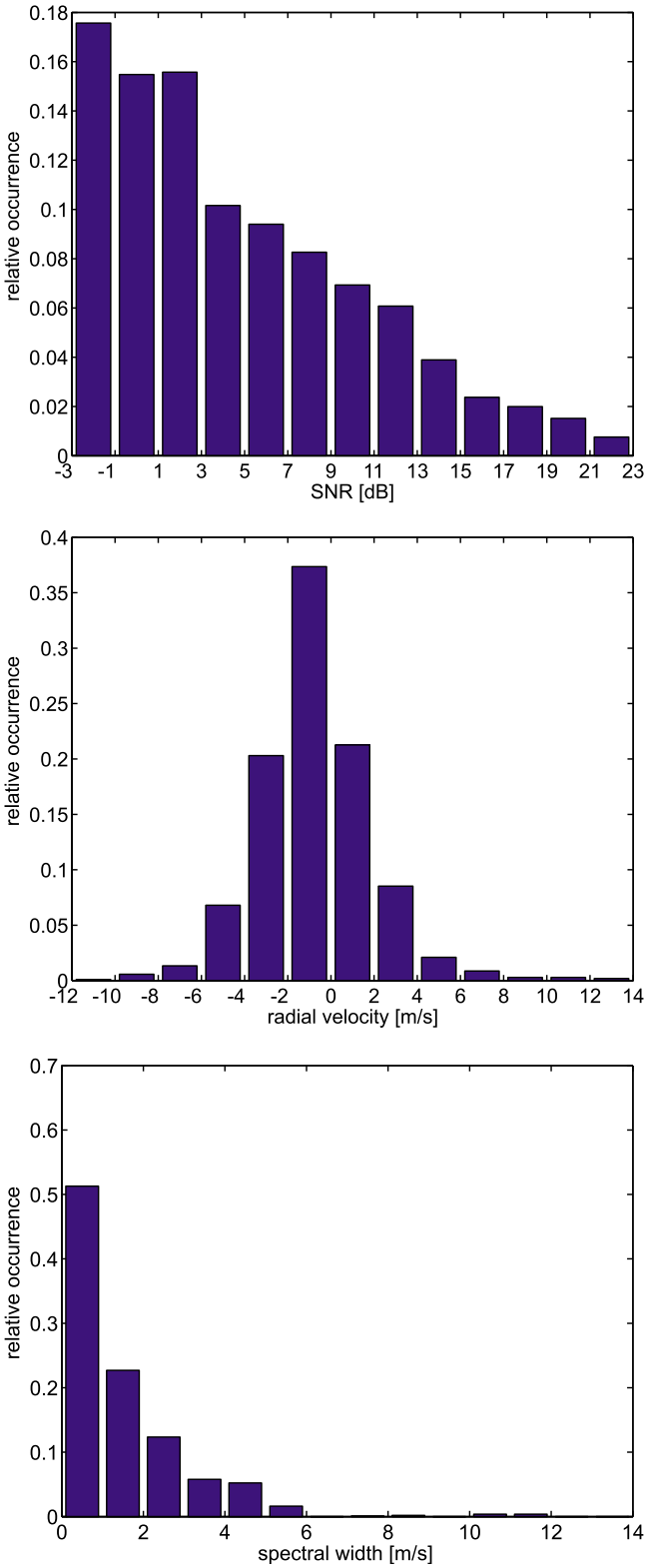

Figure 6. (top) Histograms of SNR, (middle) Doppler shift (radial velocity), and (bottom) spectral width.

et al., 2007] from June 2008 when a majority of echoes was observed. These data are overlaid in Figure 7 as contours of zonal and meridional wind values from which the mean profiles for this month were subtracted. Even though wind observations and echo occurrences only overlap at the upper edge of the wind observations for a few kilometers, Figure 7 suggests that the echo occurrences follow the phase progression of the semidiurnal tide. Interestingly, we further found that the areas of overlap correspond to times and altitudes of large values in the vertical shear of the zonal and meridional wind (lower panels of Figure 7). We will come back to this finding in section 4 where we will discuss possible physical mechanisms explaining our observations.

4. Discussion

[19] Having described the properties of the observed *E* region echoes, we now turn to a discussion of their possible physical mechanisms. We start with a quantitative discussion of a potential turbulence-related scattering mechanism similar to the processes leading to PMSE which was proposed by *Kelley* [2004] to explain so-called long-duration meteor trails. After this, we briefly turn to a discussion of field aligned irregularities from a plasma instability and finally we consider the relation of the observed echoes to sporadic layers and investigate whether the echoes could possibly results from partial reflections from the electron density gradients in very strong sporadic *E* layers.

4.1. Turbulence-Related Scatter

[20] We start with a discussion of a PMSE-like mechanism involving turbulence in connection with a large Schmidt number owing to the presence of charged heavy aerosol particles. Our considerations are motivated by the fact that such a mechanism was invoked to explain a radar observation which was interpreted as an exceptionally long-duration nonspecular meteor echo [*Kelley et al.*, 1998; *Kelley*, 2004]. This echo was observed with the 53.5 MHz CUPRI radar at the Poker Flat Rocket Range and lasted for a total of 10 min. The echo occurred at about 93 km altitude in a 15° off-zenith beam direction and descended to about 91 km during the time of observation. At the same time the echo was not observed in other beam directions indicating its localized nature. Most interestingly, this meteor trail was also traversed by a sounding rocket which provided high-resolution electron density measurements from the altitude range of the trail. The corresponding power spectrum extended well to the Bragg wavelength of the CUPRI radar and exhibited all the features that are expected for high Schmidt number scatter. In consequence, *Kelley* [2004] proposed that the echo was caused by some yet unexplained turbulence which acted on charged dust particles that were directly produced in the ablating meteor train and thereby created small-scale structures at the radar Bragg scale.

[21] In order to investigate whether the same mechanism could also possibly explain the *E* region echoes presented in the current manuscript, we have calculated absolute volume reflectivities using the scattering theory recently developed by *Rapp et al.* [2008, equation (2)] for the case of PMSE. Besides from the turbulent energy dissipation rate and the Schmidt number, the corresponding expression also depends on the electron density and its vertical gradient, the kinematic viscosity of air and the Brunt frequency. An upper limit for the turbulent energy dissipation rate can be estimated from the spectral width estimates of our radar observations using an expression derived by *Hocking* [1985].

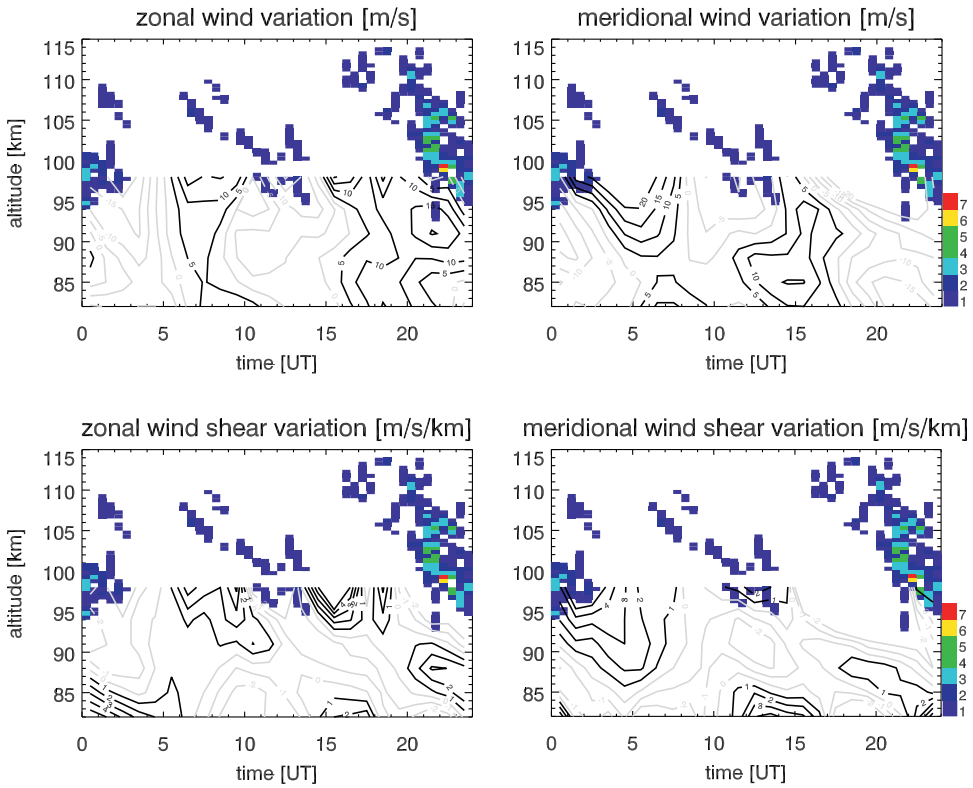

Figure 7. Number of observations as a function of time of day and altitude (color code) compared to (top left) zonal and (top right) meridional wind variations obtained from measurements with the ALOMAR Meteor radar [e.g., *Hoffmann et al.*, 2007] during June 2008 after the mean profile for this month was subtracted. Equivalent comparisons to the vertical shears of the (bottom left) zonal and (bottom right) meridional wind.

Referring back to Figure 6, we recall that the majority of observations showed spectral widths of about 1–2 m/s. Using a Brunt frequency of 0.02 s^{-1}, this corresponds to turbulent energy dissipation rates between 6 and 25 mW/kg. Note that these are upper limits for the actual dissipation rate since effects like beam, shear, and wave broadening as additional contributions to the spectral width have been ignored [*Hocking*, 1985; *Nastrom and Eaton*, 1997]. Kinematic viscosities and Brunt frequencies for different altitudes have been calculated using Sutherland's law and densities and temperatures from MSIS [*Hedin*, 1991]. Finally, electron densities and electron density gradients have been estimated on the basis of IRI-electron density profiles for the month of July and a latitude of 69°. Furthermore, a special case of a strong sporadic *E* layer (as observed by the nearby EISCAT UHF radar, see Figure 10 below and the corresponding discussion) was considered yielding a very large electron density of 2×10^{11} m^{-3} and a corresponding electron density gradient of 2×10^{8} m^{-4}. Corresponding results are presented in Figure 8. Figure 8 shows calculated volume reflectivities as a function of turbulent energy dissipation rate and particle radius *r* which determines the Schmidt number *Sc* by means of the simple relation $Sc = 6.5 \times r^2$ where *r* is given in nanometers [*Lübken et al.*, 1998; *Rapp and Lübken*, 2003]. The two upper panels show results for an altitude of 100 km with a kinematic viscosity of 56 m^2/s. Note that the observed SNRs of the echoes roughly correspond to volume reflectivities between 10^{-16} and 10^{-14} m^{-1} [*Latteck et al.*, 2008]. These calculations show that for a typical energy dissipation rate of 10 mW/kg, a particle radius of 20–25 nm could explain the weakest echoes while 22–35 nm would be needed to explain the strongest ones. We note that such large particles should actually be detectable by lidars, however, to our knowledge such observations have so far not been reported. Also, our calculations show that even much larger particles or much stronger turbulence would be needed at the upper altitudes where the echoes were observed, i.e., at and above 110 km. This is caused by the much larger kinematic viscosity of about 390 m^2/s which leads to rapid destruction of any small-scale features at these altitudes.

[22] Based on these considerations, we conclude that a turbulence with large Schmidt number related mechanism can likely be excluded as the cause of the here considered radar echoes. Nevertheless, a dedicated sounding rocket experiment to probe these echoing regions in detail like *Kelley* [2004] would be highly desirable to draw definitive conclusions.

4.2. Auroral Backscatter

[23] We next turn to the question whether the observed *E* region echoes could be caused by plasma instability-type structures caused by auroral activity. At this point it is worthwhile to remember the similarities and differences of the echoes described here and the ones discussed by *Rüster and Schlegel* [1999]. Both echoes were observed at the same geographical location and hence at almost parallel geometry

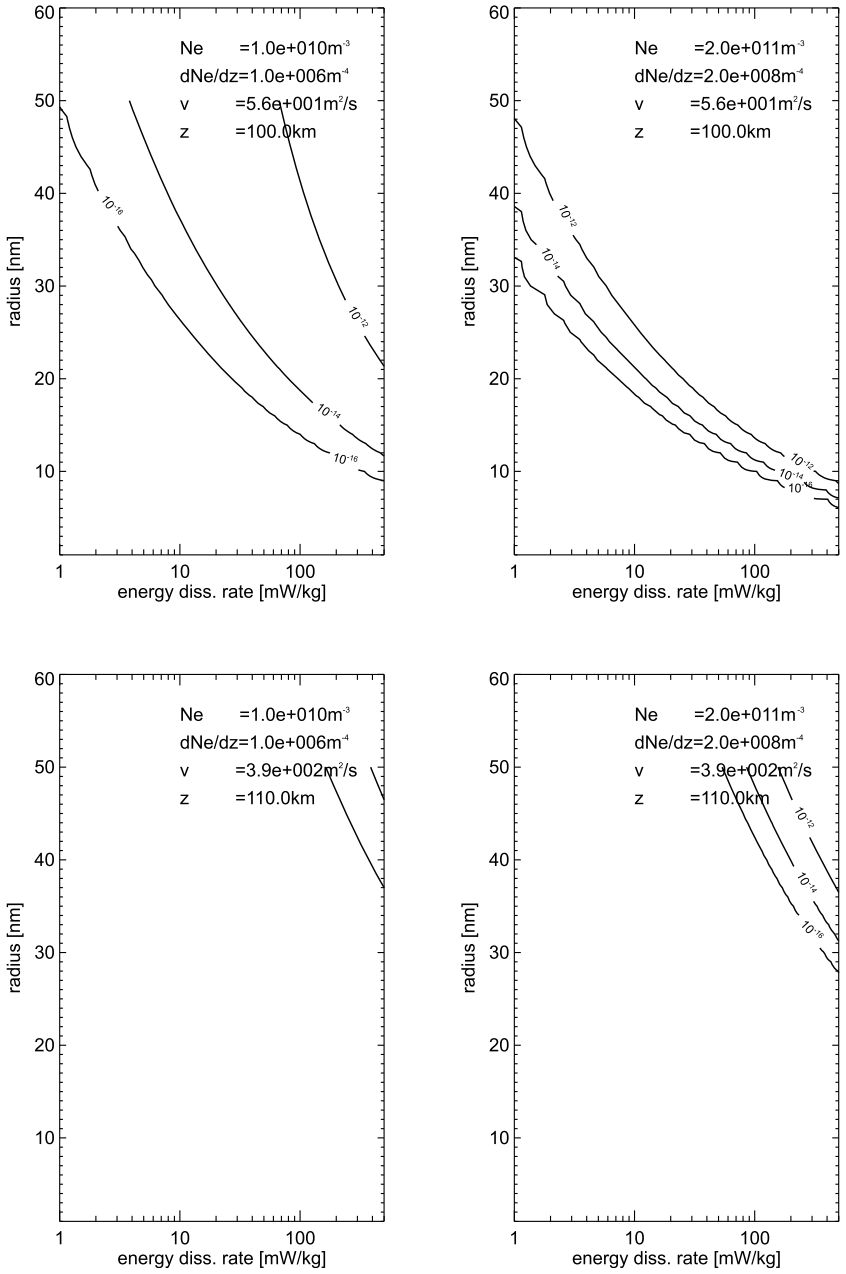

Figure 8. Theoretical values of the radar volume reflectivity (in m^{-1}) as a function of turbulent energy dissipation rate and charged particle radius for different values of the electron density and its vertical gradient and kinematic viscosity.

to the Earth's magnetic field, both echoes showed similar Doppler velocities of just a few meters per second and very narrow spectral widths and were observed in about the same overall altitude range from 90–110 km. However, the distinctive feature between both observations is that the examples shown by *Rüster and Schlegel* [1999] cover a broad altitude range of up to 15 km while our echoes typically covered only one to two range gates of 300 m each. Nevertheless, all arguments presented by *Rüster and Schlegel* [1999] against a Farley-Buneman instability or a gradient drift instability as the cause for the observed echoes also apply here and will hence not be repeated in detail. Most notably, the mechanisms stated above should lead to field aligned irregularities that should be invisible to our radar. However, in contrast to this expectation, we did not only observe the echoes at an almost parallel geometry to the geomagnetic field but furthermore observed the opposite aspect sensitivity. This means that in the vast majority of cases (93%) the echoes were only observed in the vertical beam but were not detected in the off-zenith directions in spite of considerable durations of up to ~3 h hence indicating a large spatial extent of the echoing structures. We hence conclude that our observations can likely not be explained by regular auroral backscatter. We note, however, that we can also not exclude the mechanism(s) proposed by *Robinson and Schlegel* [2000]. However, our current data-

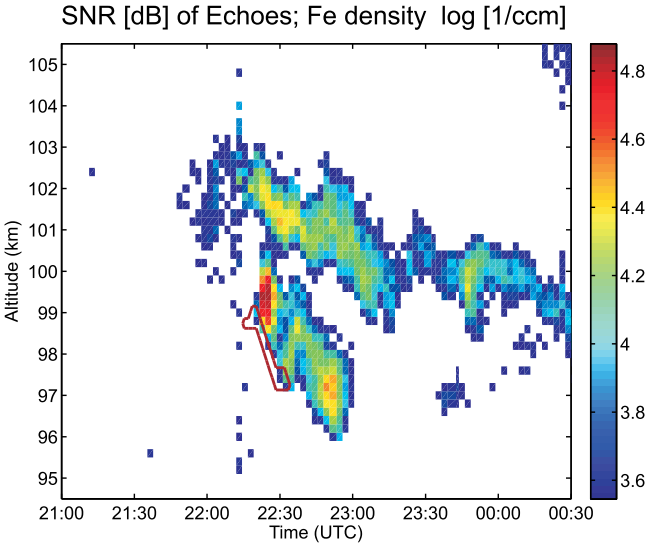

Figure 9. Simultaneous and common volume observations of atomic iron densities with the portable IAP resonance lidar (colored pixels) and the ALWIN VHF radar (red contour).

base does not allow us to check their proposal of electron drifts aligned with the geomagnetic field, neither are we in the position to speculate about the additional nonlinear feedback processes that are required in their work to shift the plasma waves into the right wavelength range. This option should be reconsidered once appropriate new data or theoretical results become available.

4.3. Partial Reflections From Electron Density Gradients in Sporadic E

[24] Finally, we consider whether the radar echoes presented here are in some way or the other related to sporadic layers, i.e., sporadic metal layers and sporadic *E* layers which were first observed in ionograms as large localized electron density enhancements and are today known to be layers of metallic ions (see, e.g., *Plane* [2003] for a review). First of all, we note that the seasonal, vertical, and diurnal occurrence of the *E* region echoes is very similar to the well known corresponding occurrence of sporadic layers at the same location. For example, *Arras et al.* [2008] presented global observations of the occurrence of sporadic *E* layers based on GPS radio occultation measurements with the CHAMP, GRACE-A and FORMOSAT-3/COSMIC satellites and found a strong seasonal variation with maximum sporadic E occurrence in summer in the altitude range from about 90 to 115 km. We note that *Haldoupis et al.* [2007] have shown that the seasonal variation of sporadic *E* layers at midlatitudes correlates so well with the seasonal variation of meteoric input, that a cause and effect relationship (via the deposition of metallic ions) seems obvious. Also, *Heinrich et al.* [2008] recently presented resonance lidar observations of the diurnal occurrence of the closely related sporadic sodium-atom layers, and found that their occurrence was concentrated at times around local midnight, i.e., from 20–02 UT. As indicated above, this is almost exactly the same seasonal, vertical, and diurnal occurrence pattern that we also observe for the *E* region radar echoes discussed in this manuscript.

[25] Furthermore, we note that the maximum of occurrence of the *E* region echoes reported here is at the time and altitude of large values of the vertical shear due to the semidiurnal tidal component of the zonal and meridional wind field (see Figure 7). This fact may suggest a relationship with one of the probable processes for sporadic E generation, i.e., the wind shear mechanism reviewed by *Mathews* [1998] and recently further discussed by *Haldoupis et al.* [2004].

[26] While this wind shear mechanism was originally proposed to explain the occurrence of sporadic *E* layers at midlatitudes where the Earth's magnetic field has a large horizontal component [*Whitehead*, 1960], it has recently been shown by *Nygrén et al.* [2008] that even a small horizontal component of the magnetic field can be sufficient for the wind shear mechanism to be active. This is also the case for instance at polar latitudes, where it is generally thought that electric fields are mainly responsible for sporadic E generation [e.g., *Nygrén et al.*, 1984; *Kirkwood and Nilsson*, 2000; *Voiculescu et al.*, 2006; *Nygrén et al.*, 2006]. Using a combination of observations with the EISCAT Svalbard Radar and numerical modeling, *Nygrén et al.* [2008] were able to demonstrate that depending on the specific situation, sporadic E generation in the polar cap can be mainly attributed to the wind shear mechanism, to the electric field mechanism, or to the combined effect of both.

[27] To compare our results with these published findings and suggested mechanisms, we checked whether the closest ionosonde observations with the Tromsø dynasonde [*Rietveld et al.*, 2008] provided evidence for the occurrence of sporadic *E* layers at the times when *E* region echoes were recorded with the ALWIN radar at a horizontal distance of about 130 km. Indeed, we found that during the vast majority of our observations, the Tromsø dynasonde did observe sporadic *E* layers, further supporting the view that the *E* region echoes were somehow related to sporadic *E* layers.

[28] In fact, we are able to present further support for this hypothesis in the form of simultaneous and common volume measurements of a sporadic Fe layer with the transportable Fe resonance lidar of the IAP [*Höffner and Lautenbach*, 2009] and one of the *E* region radar echoes discussed in this manuscript. The corresponding observations are presented in Figure 9. Figure 9 shows color-coded Fe number densities according to which a sporadic Fe layer occurred shortly before 22 UT on 7 July 2008. Right at the time when the sporadic layer reached an altitude of about 99 km, the radar echo appeared (red contour lines) and lasted for the next ~30 min. Note that the lidar measurements also allow us to rule out contributions from Mie scattering by large aerosol particles since the prime purpose of these lidar measurements is to derive temperatures from scanning the iron resonance line at 386 nm. Routinely, this scan is extended far out into the wings of the resonance line where contributions from Mie scattering should be easily recognized [see *Höffner and Lautenbach*, 2009, Figure 4]. Inspection of the corresponding features for the observations presented here proves that no detectable contribution from Mie scattering owing to the presence of large aerosol particles was observed. This is further support for our earlier statement that turbulence with large Schmidt number scatter can likely be excluded as the cause for the observed MST radar echoes.

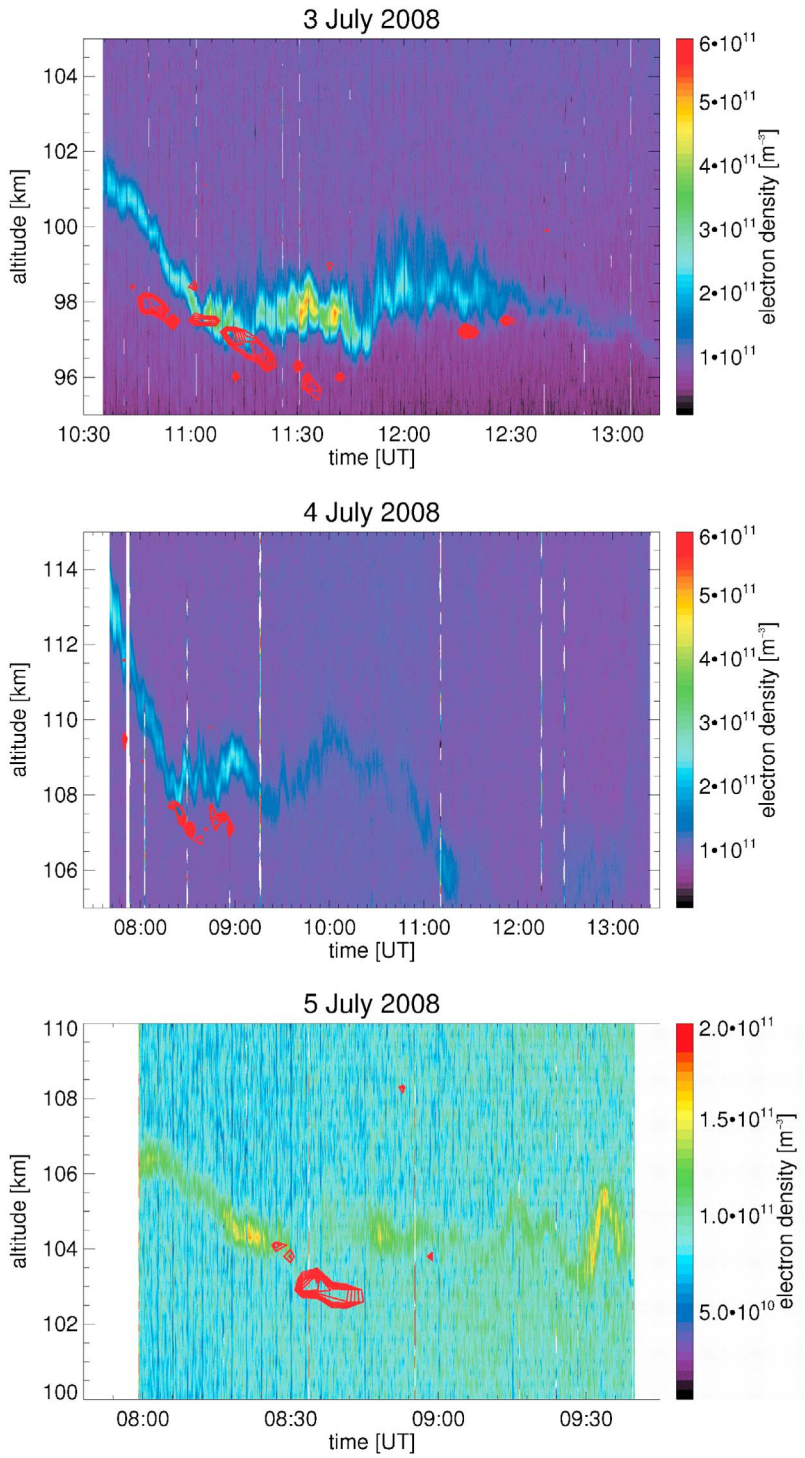

Figure 10. Simultaneous observations of electron densities with the EISCAT UHF radar in Tromsø and of *E* region radar echoes with the ALWIN VHF radar at Andenes (red contour lines), i.e., 130 km apart, on (top) 3 July, (middle) 4 July, and (bottom) 5 July 2008.

[29] Finally, we also considered whether direct observations of *E* region electron densities had been obtained with the EISCAT radars in Tromsø at the times when ALWIN recorded the *E* region radar echoes. Indeed, such measurements were obtained on 3–5 July 2008 with the EISCAT UHF radar using the "arc-dlayer" experiment [*Baron*, 1986; *Turunen et al.*, 2002]. This experiment provides electron density profiles in the relevant altitude range at 300 m vertical resolution. An overview of these measurements together with the simultaneously observed *E* region VHF radar echoes is presented in Figure 10. This reveals that the *E* region VHF radar echoes indeed occurred in the presence

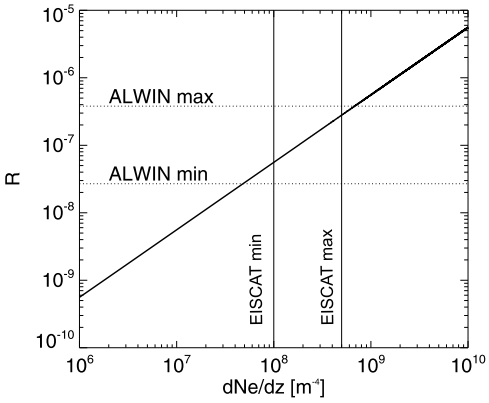

Figure 11. Calculations of reflection coefficients as a function of electron density gradient. Dotted horizontal lines indicate the range of reflection coefficients derived from the ALWIN observations, and the vertical solid lines indicate the minimum and maximum electron density gradients as derived from EISCAT observations of sporadic *E* layers during ALWIN observations of *E* region radar echoes.

of sporadic *E* layers. However, we also need to consider some obvious differences. First of all, we note that the altitudes and times of the two echo types did not coincide perfectly, as they did in the case of the simultaneous and common volume measurements with the Fe lidar. However, this can probably be explained by the fact that the EISCAT measurements were taken at a horizontal distance of about 130 km such that a perfect match between the EISCAT measurements at Tromsø and the MST radar measurements at ALOMAR can actually not be expected. In addition, we note that the MST radar echoes lasted for considerably shorter times than the sporadic *E* layers; that is, the MST radar echoes lasted between 15 min and 1 h, while the corresponding sporadic *E* layers lasted between 1 and 2 h. Despite of these differences, we take these observations as additional support for our hypothesis of a close relation between sporadic *E* layers and *E* region MST radar echoes.

[30] So what could be the relation between these two phenomena? First of all, we note that the MST radar echoes can certainly not have originated from total reflection since a plasma frequency of 50 MHz corresponds to an electron density of 3.1×10^{13} m^{-3} which is almost 2 orders of magnitude larger than the maximum electron densities observed with the EISCAT UHF radar as presented in Figure 10. Next, we note that sporadic E-related plasma irregularities as reported for example by *Hysell et al.* [2009] should lead to field-aligned irregularities and should hence be invisible to our radar (see also the discussion of auroral backscatter above).

[31] Hence, the final possibility that we consider in this study is partial reflections from the electron density gradients in sporadic *E* layers. Partial reflections have been studied for many years and were successfully shown to account for HF radar echoes [e.g., *Thrane et al.*, 1968, 1981; *Belrose et al.*, 1972; *Meek and Manson*, 1981; *Hocking and Vincent*, 1982] while it was argued that it is very unlikely that partial reflections could also account for the very strong VHF radar echoes known as PMSE simply because of the much smaller spatial scales involved [*Hocking and Röttger*, 1997]. However, the latter authors did not consider the very large electron density gradients which could occur in sporadic *E* layers which could possibly lead to corresponding large changes in the electron density over such small vertical extents of only half a radar wavelength, i.e., only 2.8 m in the case of the ALWIN radar.

[32] In order to test whether the electron density gradients corresponding to the observations shown in Figure 10 could have caused partial reflections that were then recorded by the ALWIN radar, we have followed the derivation of *Hocking and Röttger* [1997] to calculate the reflection coefficient. This exercise yields

$$R = \frac{1}{2} \cdot \frac{dN_e}{dz} \cdot d \cdot \frac{r_e \lambda^2}{2\pi} \cdot \exp\left(-\frac{\pi^2 \xi^2 d^2}{4 \ln(2)}\right) \quad (1)$$

where N_e is the electron density and dN_e/dz is its vertical gradient. d is the vertical step size over which the electron density change is considered. For the current purpose, we set this to half the radar wavelength, i.e., to $\lambda/2$ since it was pointed out by *Hocking and Röttger* [1997] that steps need to be of that size or shorter in order to allow specular reflections to result in detectable echoes. r_e is the classical electron radius, and $\xi = 2/\lambda$.

[33] As a next step we have derived electron density gradients from the EISCAT measurements of sporadic *E* layers shown in Figure 10. This yields values between $1–5 \times 10^8$ m^{-4} (or $1–5 \times 10^{11}$ m^{-3}/km). Using this range of values in equation (1), we obtain reflection coefficients between $R = 6 \times 10^{-8}$ and $R = 4 \times 10^{-7}$. So how does this compare to our radar measurements? Again, we follow *Hocking and Röttger* [1997] according to which volume reflectivities obtained under the assumption of volume scattering instead of partial reflections can be converted to reflection coefficients by means of

$$\langle R^2 \rangle = \eta \theta_{1/2}^2 L \quad (2)$$

where η is the volume reflectivity, L is the radar pulse length, and $\theta_{1/2}$ is the half power half width of the radar beam. Using the calibration of the ALWIN radar described by *Latteck et al.* [2008], we derive that the SNR values presented in Figure 6 correspond to volume reflectivities between 2.2×10^{-16} m^{-1} and 4.4×10^{-14} m^{-1}. Using further a pulse length $L = 300$ m and $\theta_{1/2} = 3$ deg, we see that this corresponds to reflection coefficients between $R = 2.6 \times 10^{-8}$ and $R = 5.2 \times 10^{-7}$. Comparing these values to our theoretical estimates above, we find that the values closely match (see also Figure 11). It hence appears that partial reflections can indeed explain the observed MST radar echoes.

5. Conclusions

[34] In the current manuscript we have presented the first observations, to our knowledge, of a new class of high-latitude MST radar echoes from the *E* region. During the years 2004–2008 the echoes were observed with the ALOMAR wind radar (69°N, 16°E) during a total of 59 h. The echoes occurred primarily, though not exclusively,

during the summer months and in the altitude range from 93–114 km with a pronounced peak of maximum occurrence at about 100 km. The echoes were rather short with typical durations of ~20 min with some examples lasting as long as 3 h. The vertical extent of the echoes typically covered only 1–2 range gates (of 300 m length each) and never exceeded three range gates. SNR varied between −3 dB and +23 dB and analysis of Doppler spectra showed that typical vertical velocities were about ±1–2 m/s with an average downward speed of ~−1 m/s. Corresponding spectral widths were very small with typical values of just a few meters per second. Also, the echoes appeared to be highly aspect sensitive; that is, only in a few cases echoes were observed in off-zenith directions. In addition, the echoes revealed a strong semidiurnal variation with maxima of occurrence around noon and midnight. In the altitude range of overlap, analysis of zonal and meridional wind measurements with a collocated MF radar revealed that altitudes and times of occurrence corresponded to large values in the vertical shear of the semidiurnal tidal component of the zonal and meridional wind. Considering next possible physical mechanisms, turbulence with large Schmidt number related scatter was likely ruled out, as was auroral scatter. Turning finally to a possible relation of the echoes to sporadic *E* layers a strong case for their close correspondence could be presented based on comparisons to ionosonde data, occurrence patterns, simultaneous and common volume lidar measurements of a sporadic Fe layer, as well as direct measurements of sporadic *E* layers with the EISCAT UHF radar at a horizontal distance of 130 km. Applying the theory of partial reflections to the observed electron density gradients, we were able to demonstrate that the observed echo strengths can likely be quantitatively explained on the basis of this scattering mechanism.

[35] For the future, an even stronger case for or against this mechanism should be made by means of real common volume measurements of electron densities and MST radar echoes. This should be possible in the near future making use of the MORRO MST radar which is collocated with the EISCAT VHF and UHF radars [e.g., *La Hoz and Havnes*, 2008]. Ideally, such new observations should also be designed to identify the cause of the underlying sporadic *E* layer and clarify whether state-of-the-art theory of these layers can actually explain the very large gradients that apparently cause the *E* region echoes presented here. Further points for future investigations are the peculiar year-to-year variation seen in the ALWIN data (i.e., a steady increase of observations from 2004 to 2008) as well as a possible latitudinal variation of these echoes since global observations of sporadic *E* layers from satellites suggest a maximum of occurrence at midlatitudes [*Arras et al.*, 2008]. The analysis of corresponding observations at 55°N using the OSWIN radar at Kühlungsborn, Germany [e.g., *Zecha et al.*, 2003] has just been started and will be presented in a future publication.

[36] **Acknowledgments.** The availability of EISCAT dynasonde data for this study is greatly appreciated. EISCAT is an international association supported by research organizations in China (CRIRP), Finland (SA), France (CNRS, until end 2006), Germany (DFG, formerly MPG), Japan (NIPR and STEL), Norway (NFR), Sweden (VR), and the United Kingdom (PPARC).

[37] Robert Lysak thanks Sixto Gonzalez and another reviewer for their assistance in evaluating this paper.

References

Arras, C., J. Wickert, G. Beyerle, S. Heise, T. Schmidt, and C. Jacobi (2008), A global climatology of ionospheric irregularities derived from GPS radio occultation, *Geophys. Res. Lett.*, *35*, L14809, doi:10.1029/2008GL034158.

Baron, M. (1986), EISCAT progress 1983–1985, *J. Atmos. Terr. Phys.*, *48*, 767–772.

Belova, E., S. Kirkwood, J. Ekeberg, A. Osepian, H. N. I. Häggström, and M. Rietveld (2005), The dynamical background of polar mesosphere winter echoes from simultaneous EISCAT and ESRAD observations, *Ann. Geophys.*, *23*, 1239–1247.

Belrose, J. S., M. J. Burke, T. N. R. Coyne, and J. E. Reed (1972), D-region measurements with the differential-absorption, differential-phase partial-reflection experiments, *J. Geophys. Res.*, *77*, 4829–4838.

Brattli, A., T. A. Blix, O. Lie-Svendsen, U.-P. Hoppe, F.-J. Lübken, M. Rapp, W. Singer, R. Latteck, and M. Friedrich (2006), Rocket measurements of positive ions during polar mesosphere winter echo conditions, *Atmos. Chem. Phys.*, *6*, 5515–5524.

Cho, J. Y., and M. C. Kelley (1993), Polar mesosphere summer radar echoes, *Rev. Geophys.*, *31*, 243–265.

Cho, J. Y. N., T. M. Hall, and M. C. Kelley (1992), On the role of charged aerosols in polar mesosphere summer echoes, *J. Geophys. Res.*, *97*, 875–886.

Czechowsky, P., R. Rüster, and G. Schmidt (1979), Variations of mesospheric structures in different seasons, *Geophys. Res. Lett.*, *6*, 459–462.

Ecklund, W. L., and B. B. Balsley (1981), Long-term observations of the arctic mesosphere with the MST radar at Poker Flat, Alaska, *J. Geophys. Res.*, *86*, 7775–7780.

Friedrich, M., and M. Rapp (2009), News from the lower ionosphere: A review of recent developements, *Surv. Geophys.*, *30*, 525–559, doi:10.1007/s1071200990742.

Haldoupis, C. (1989), A review on radio studies of auroral E-region ionospheric irregularities, *Ann. Geophys.*, *7*, 239–258.

Haldoupis, C., D. Pancheva, and N. J. Mitchell (2004), A study of tidal and planetary wave periodicities present in midlatitude sporadic E-layers, *J. Geophys. Res.*, *109*, A02302, doi:10.1029/2003JA010253.

Haldoupis, C., D. Pancheva, W. Singer, C. Meek, and J. MacDougall (2007), An explanation for the seasonal dependence of midlatitude sporadic E-layers, *J. Geophys. Res.*, *112*, A06315, doi:10.1029/2007JA012322.

Havnes, O., J. Trøim, T. Blix, W. Mortensen, L. I. Næsheim, E. Thrane, and T. Tønnesen (1996), First detection of charged dust particles in the Earth's mesosphere, *J. Geophys. Res.*, *101*, 10,839–10,847.

Hedin, A. E. (1991), Extension of the MSIS thermosphere model into the middle and lower atmosphere, *J. Geophys. Res.*, *96*, 1159–1172.

Heinrich, D., H. Nesse, U. Blum, P. Acott, B. Williams, and U.-P. Hoppe (2008), Summer sudden Na number density enhancements measured with the ALOMAR Weber Na Lidar, *Ann. Geophys.*, *26*, 1057–1069.

Hocking, W. (2011), A review of mesosphere-stratosphere-troposphere (MST) radar developments and studies, circa 1997–2008, *J. Atmos. Sol. Terr. Phys.*, doi:10.1016/j.jastp.2010.12.009, in press.

Hocking, W. K. (1985), Measurement of turbulent energy dissipation rates in the middle atmosphere by radar techniques: A review, *Radio Sci.*, *20*, 1403–1422.

Hocking, W. K., and J. Röttger (1997), Studies of polar mesosphere summer echoes over EISCAT using calibrated signal strengths and statistical parameters, *Radio Sci.*, *32*, 1425–1444.

Hocking, W. K., and R. A. Vincent (1982), A comparison between HF partial reflection profiles from the D-region and simultaneous Langmuir probe electron density measurements, *J. Atmos. Terr. Phys.*, *44*, 843–854.

Hoffmann, P., W. Singer, D. Keuer, W. K. Hocking, M. Kunze, and Y. Murayama (2007), Latitudinal and longitudinal variability of mesospheric winds and temperatures during stratospheric warming events, *J. Atmos. Sol. Terr. Phys.*, *69*, 2355–2366.

Höffner, J., and J. Lautenbach (2009), Daylight measurements of mesopause temperature and vertical wind with the mobile scanning iron lidar, *Optics Lett.*, *34*, 1351–1353.

Hoppe, U.-P., and T. Hansen (1988), Studies of vertical motions in the upper mesosphere using the EISCAT UHF radar, *Ann. Geophys.*, *6*, 181–186.

Hysell, D. L., E. Nossa, M. F. Larsen, J. Munro, M. P. Sulzer, and S. A. Gonzalez (2009), Sporadic E layer observations over Arecibo using coherent and incoherent scatter radar: Assessing dynamic stability in the lower thermosphere, *J. Geophys. Res.*, *114*, A12303, doi:10.1029/2009JA014403.

Kelley, M. C. (2004), A new explanation for long-duration meteor radar echoes: Persistent charged dust trains, *Radio Sci.*, *39*, RS2015, doi:10.1029/2003RS002988.

Kelley, M. C., D. T. Farley, and J. Röttger (1987), The effect of cluster ions on anomalous VHF backscatter from the summer polar mesosphere, *Geophys. Res. Lett.*, *14*, 1031–1034.

Kelley, M. C., C. Alcala, and J. Y. N. Cho (1998), Detection of a meteor contrail and meteoric dust in the Earth's upper mesosphere, *J. Atmos. Sol. Terr. Phys.*, *60*, 359–369.

Kirkwood, S., and H. Nilsson (2000), High-latitude sporadic-E and other thin layers: The role of magnetospheric electric fields, *Space Sci. Rev.*, *91*, 579–613.

Kirkwood, S., V. Barabash, E. Belova, H. Nilsson, N. Rao, K. Stebel, A. Osepian, and P. B. Chilson (2002), Polar mesosphere winter echoes during solar proton events, *Adv. Pol. Up. Atmos. Res.*, *16*, 111–125.

Kirkwood, S., P. Chilson, E. Belova, P. Dalin, I. Häggström, M. Rietveld, and W. Singer (2006), Infrasound–the cause of strong polar mesosphere winter echoes?, *Ann. Geophys.*, *24*, 475–491.

La Hoz, C., and O. Havnes (2008), Artificial modification of polar mesospheric winter echoes with an RF heater: Do charged dust particles play an active role?, *J. Geophys. Res.*, *113*, D19205, doi:10.1029/2008JD010460.

Latteck, R., W. Singer, and H. Bardey (1999), The ALWIN MST radar: Technical design and performance, in *Proceedings of the 14th ESA Symposium on European Rocket and Balloon Programmes and Related Research, Potsdam, Germany*, *Eur. Space Agency Spec. Publ.*, *ESA SP-437*, pp. 179–184.

Latteck, R., W. Singer, R. J. Morris, D. A. Holdsworth, and D. J. Murphy (2007), Observation of polar mesosphere summer echoes with calibrated VHF radars at 69° in the Northern and Southern Hemisphere, *Geophys. Res. Lett.*, *34*, L14805, doi:10.1029/2007GL030032.

Latteck, R., W. Singer, R. J. Morris, W. K. Hocking, D. J. Murphy, D. A. Holdsworth, and N. Swarnalingam (2008), Similarities and differences in polar mesosphere summer echoes observed in the arctic and antarctica, *Ann. Geophys.*, *26*, 2795–2806.

Li, Q., M. Rapp, J. Röttger, R. Latteck, M. Zecha, I. Strelnikova, G. Baumgarten, M. Hervig, and C. Hall (2010), Microphysical parameters of mesospheric ice clouds derived from calibrated observations of polar mesosphere summer echoes at Bragg wavelengths of 2.8 m and 30 cm, *J. Geophys. Res.*, *115*, D00I13, doi:10.1029/2009JD012271.

Lie-Svendsen, O., T. A. Blix, U. Hoppe, and E. Thrane (2003), Modelling the plasma response to small-scale particle perturbations in the mesopause region, *J. Geophys. Res.*, *108*(D8), 8442, doi:10.1029/2002JD002753.

Lübken, F.-J. (1999), Thermal structure of the Arctic summer mesosphere, *J. Geophys. Res.*, *104*, 9135–9149.

Lübken, F.-J., M. Rapp, T. Blix, and E. Thrane (1998), Microphysical and turbulent measurements of the Schmidt number in the vicinity of polar mesosphere summer echoes, *Geophys. Res. Lett.*, *25*, 893–896.

Lübken, F.-J., B. Strelnikov, M. Rapp, W. Singer, R. Latteck, A. Brattli, U.-P. Hoppe, and M. Friedrich (2006), The thermal and dynamical state of the atmosphere during polar mesosphere winter echoes, *Atmos. Chem. Phys.*, *5*, 13–24.

Lübken, F.-J., W. Singer, R. Latteck, and I. Strelnikova (2007), Radar measurements of turbulence, electron densities, and absolute reflectivities during polar mesosphere winter echoes (PMWE), *Adv. Space Res.*, *40*, 758–764, doi:10.1016/j.asr.2007.01.015.

Mathews, J. (1998), Sporadic E: Current views and recent progress, *J. Atmos. Sol. Terr. Phys.*, *60*, 413–435.

Meek, C. E., and A. H. Manson (1981), Use of the full polarization measurement in the partial reflection experiment, *J. Atmos. Terr. Phys.*, *43*, 45–58.

Nastrom, G. D., and F. D. Eaton (1997), Turbulence eddy dissipation rates from radar observations at 5–20 km at White Sands Missile Range, New Mexico, *J. Geophys. Res.*, *102*, 19,495–19,505.

Nicolls, M. J., M. C. Kelley, R. H. Varney, and C. J. Heinselman (2008), Spectral observations of polar mesospheric summer echoes at 33 cm (450 MHz) with the Poker Flat incoherent scatter radar, *J. Atmos. Sol. Terr. Phys.*, *71*, 662–674.

Nygrén, T., L. Jalonen, J. Oksman, and T. Turunen (1984), The role of electric field and neutral wind direction in the formation of sporadic E-layers, *J. Atmos. Terr. Phys.*, *46*, 373–381.

Nygrén, T., A. T. Aikio, M. Voiculescu, and J. M. Ruohoniemi (2006), IMF effect on sporadic-E layers at two northern polar cap sites: Part II - Electric field, *Ann. Geophys.*, *24*, 901–913, doi:10.5194/angeo-249012006.

Nygrén, T., M. Voiculescu, and A. T. Aikio (2008), The role of electric field and neutral wind in the generation of polar cap sporadic E, *Ann. Geophys.*, *26*, 3757–3763, doi:10.5194/angeo-2637572008.

Plane, J. M. C. (2003), Atmospheric chemistry of meteoric metals, *Chem. Rev.*, *103*, 4963–4984.

Rapp, M., and F.-J. Lübken (2003), On the nature of PMSE: Electron diffusion in the vicinity of charged particles revisited, *J. Geophys. Res.*, *108*(D8), 8437, doi:10.1029/2002JD002857.

Rapp, M., and F.-J. Lübken (2004), Polar mesosphere summer echoes (PMSE): Review of observations and current understanding, *Atmos. Chem. Phys.*, *4*, 2601–2633.

Rapp, M., I. Strelnikova, R. Latteck, P. Hoffmann, U.-P. Hoppe, I. Häggström, and M. Rietveld (2008), Polar mesospher summer echoes (PMSE) studied at bragg wavelengths of 2.8 m, 67 cm, and 16 cm, *J. Atmos. Sol. Terr. Phys.*, *70*, 947–961, doi:10.1016/j.jastp.2007.11.005.

Rietveld, M., J. Wright, N. Zabotin, and M. Pitteway (2008), The Tromsø dynasonde, *Polar Sci.*, *2*, 55–71.

Robinson, T. R., and K. Schlegel (2000), The generation of non aspect sensitive plasma density irregularities by field aligned drifts in the lower ionosphere, *Ann. Geophys.*, *18*, 799–806.

Rüster, R., and K. Schlegel (1999), Non-magnetic aspect sensitive auroral echoes from the lower E region observed at 50 MHz, *Ann. Geophys.*, *17*, 1284–1292.

Thrane, E. V., A. Haug, B. Bejelland, M. Anastassidades, and E. Tsagakis (1968), Measurements of D-region electron densities during the international quiet sun years, *J. Atmos. Terr. Phys.*, *30*, 135–150.

Thrane, E. V., B. Grandal, T. Fla, and A. Brekke (1981), Fine structure in the ionospheric D-region, *Nature*, *292*, 221–223.

Turunen, T., A. Westman, I. Häggström, and G. Wannberg (2002), High resolution general purpose D-layer experiment for EISCAT incoherent scatter radars using selected set of random codes, *Ann. Geophys.*, *20*, 1469–1477.

Varney, R. H., M. C. Kelley, M. J. Nicolls, C. J. Heinselman, and R. L. Collins (2011), The electron density dependence of polar mesospheric summer echoes, *J. Atmos. Sol. Terr. Phys.*, doi:10.1016/j.jastp.2010.07.020, in press.

Voiculescu, M., A. T. Aikio, T. Nygrén, and J. M. Ruohoniemi (2006), IMF effect on sporadic-E layers at two northern polar cap sites: Part I – Statistical study, *Ann. Geophys.*, *24*, 887–900, doi:10.5194/angeo-248872006.

Whitehead, J. D. (1960), Formation of the sporadic E layer in the temperate zones, *Nature*, *188*, 567.

Woodman, R. F., and A. Guillen (1974), Radar observations of winds and turbulence in the stratosphere and mesosphere, *J. Atmos. Sci.*, *31*, 493–505.

Zecha, M., J. Bremer, R. Latteck, and W. Singer (2003), Properties of midlatitude mesosphere summer echoes after three seasons of VHF radar observations at 54°N, *J. Geophys. Res.*, *108*(D8), 8439, doi:10.1029/2002JD002442.

Zeller, O., M. Zecha, J. Bremer, R. Latteck, and W. Singer (2006), Mean characteristics of mesosphere winter echoes at mid- and high-latitudes, *J. Atmos. Sol. Terr. Phys.*, *68*, 1087–1104.

P. Hoffmann, J. Höffner, R. Latteck, L. Leitert, M. Rapp, and M. Zecha, Leibniz Institute of Atmospheric Physics at University of Rostock, Schlossstr. 6, D-18225 Kühlungsborn, Germany. (rapp@iap-kborn.de)

U.-P. Hoppe, Norwegian Defense Research Establishment, PO Box 25, N-2007 Kjeller, Norway.

C. La Hoz, Department of Physics, University of Tromsø, N-9037 Tromsø, Norway.

E. V. Thrane, Andøya Rocket Range, PO Box 54, N-8483 Andenes, Norway.